



1 Kinetics and impacting factors of HO₂ uptake onto submicron atmospheric aerosols during a
2 2019 air quality study (AQUAS) in Yokohama, Japan

3 Jun Zhou^{a,b,c,*}, Kei Sato^d, Yu Bai^e, Yukiko Fukusaki^f, Yuka Kousa^f, Sathiyamurthi Ramasamy^d,
4 Akinori Takami^d, Ayako Yoshino^d, Tomoki Nakayama^g, Yasuhiro Sadanaga^h, Yoshihiro
5 Nakashimaⁱ, Jiaru Li^c, Kentaro Murano^c, Nanase Kohno^c, Yosuke Sakamoto^{c,d,e}, Yoshizumi
6 Kajii^{c,d,e,*}

7 ^aInstitute for Environmental and Climate Research, Jinan University, 511443 Guangzhou, China

8 ^bGuangdong-Hongkong-Macau Joint Laboratory of Collaborative Innovation for Environmental Quality,
9 Guangzhou 511443, China

10 ^cGraduate School of Global Environmental Studies, Kyoto University, Kyoto, 606-8501, Japan

11 ^dCenter for Regional Environmental Research, National Institute for Environmental Studies, Tsukuba,
12 Ibaraki 305-8506, Japan

13 ^eGraduate School of Human and Environmental Studies, Kyoto University, Kyoto 606-8501, Japan

14 ^fYokohama Environmental Science Research Institute, Yokohama Kanagawa 221-0024, Japan

15 ^gFaculty of Environmental Science and Graduate School of Fisheries and Environmental Sciences, Nagasaki
16 University, Nagasaki 852-8521, Japan

17 ^hGraduate School of Engineering, Osaka Prefecture University, Sakai, Osaka 599-8531, Japan

18 ⁱGraduate School of Agriculture, Tokyo University of Agriculture and Technology, 3-5-8 Saiwai-cho, Fuchu,
19 Tokyo 183-8538, Japan

20 *Corresponding author.

21 Graduate School of Global Environmental Studies, Kyoto University, Kyoto 606-8501, Japan

22 E-mail address: kajii.yoshizumi.7e@kyoto-u.ac.jp and junzhou@jnu.edu.cn

23

24

25

26

27



28 Abstract

29 HO₂ uptake kinetics onto ambient aerosols play pivotal roles in tropospheric chemistry but are not fully
30 understood. Field measurements of aerosol chemical and physical properties should be linked to
31 molecular level kinetics; however, given that the HO₂ reactivity of ambient aerosols is low, traditional
32 analytical techniques are unable to achieve this goal. We developed an online approach to precisely
33 investigate (i) the HO₂ reactivity of ambient gases and aerosols and (ii) HO₂ uptake coefficients onto
34 ambient aerosols (γ) during 2019 air quality study (AQUAS) in Yokohama, Japan. We identified the
35 effects of individual chemical components of ambient aerosols on γ . The results verified in laboratory
36 studies on individual chemical components: transition metals play a key role in HO₂ uptake processes
37 and chemical components indirectly influence such processes (i.e., through altering aerosol surface
38 properties or providing active sites), with smaller particles tending to yield higher γ values than larger
39 particles owing to the limitation of gas phase diffusion is smaller with micrometer particles and the
40 distribution of depleting species such as transition metal ions is mostly distributed in accumulation
41 mode of aerosol. The modeling of γ utilized transition metal chemistry derived by previous studies,
42 further confirming our conclusion. However, owing to the high NO concentrations in Yokohama, peroxy
43 radical loss onto submicron aerosols has a negligible impact on O₃ production rate and sensitivity
44 regime.

45 1 Introduction

46 As an important atmospheric trace gas, the hydroperoxyl radical (HO₂) links many of the key oxidants
47 in the troposphere, including the hydroxyl radical (OH), nitrate radical (NO₃⁻), ozone (O₃), and
48 hydrogen peroxide (H₂O₂) (Logan et al., 1981; Chen et al., 2001; Jaeglé et al., 2000; Sommariva et al.,
49 2004; Jacob, 2000). However, its observed concentration in field measurements has not yet been fully
50 explained by sophisticated models (known as the “HOx dilemma”) (Stone et al., 2012; Creasey et al.,
51 1997; Kanaya et al., 2007b; Whalley et al., 2010; Millán et al., 2015), although it can be mostly solved
52 in the conditions of clean marine air or stratospheric air where NO concentration is low or aerosol



53 loading is low enough to make the heterogeneous reaction of HO₂ not important (Sommariva et al.,
54 2004; Kanaya et al., 2007a). Owing to the short atmospheric lifetime of HO_x(=OH+HO₂+RO₂), the
55 HO_x reactivity measurement can provide a robust test of its complex chemistry (Heard and Pilling,
56 2003). The HO₂ uptake kinetics of ambient aerosols, including HO₂ reactivity (k_a) and the HO₂ uptake
57 coefficient (γ), influence many atmospheric processes, including ozone formation rates and their
58 sensitivity to NO_x (Sakamoto et al., 2019), H₂O₂ formation thus aerosol properties (Thornton et al.,
59 2008). With $\gamma > 0.1$, HO₂ concentration can also be influenced under conditions such as low [NO] or
60 high aerosol loading (Lakey et al., 2015; Mao et al., 2013b; Martínez et al., 2003; Tie et al., 2001, Jacob,
61 2000; Matthews et al., 2014). These effects make the HO₂ uptake kinetics of ambient aerosols indirectly
62 influence human health and climate change.

63 From laboratory, field, and modeling studies (Taketani et al., 2012; Taketani et al., 2008;
64 Bedjanian et al., 2005; Thornton et al., 2008; George et al., 2013; Lakey et al., 2016a; Lakey et al.,
65 2016b; Matthews et al., 2014; Cooper and Abbatt, 1996; Hanson et al., 1992; Thornton and Abbatt,
66 2005; González Palacios et al., 2016; Mozurkewich et al., 1987; Remorov et al., 2002; Jaeglé et al.,
67 2000; Loukhovitskaya et al., 2009; Stone et al., 2012), HO₂ uptake coefficients onto different types of
68 aerosol can span several orders of magnitude (~0.002–1), which can be affected by many parameters,
69 such as droplet/particle size and composition, the presence of dissolved reactive gases (Mozurkewich
70 et al., 1987), and environmental conditions (i.e., relative humidity (RH), pH, and T). In the absence of
71 metals, the uptake of HO₂ by ambient aerosols is believed to occur *via* the acid–base dissociation of
72 HO₂ ($pK_a = 4.7$), followed by electron transfer from O₂⁻ to HO₂ (aq), producing H₂O₂ (Jacob, 2000;
73 Thornton et al., 2008; Zhou et al., 2019b). However, laboratory studies have shown that certain
74 transition metals (i.e., Cu(II) and Fe(II)) can act as catalysts and accelerate HO₂ uptake rates onto many
75 chemical compounds (Thornton et al., 2008; Taketani et al., 2008; Taketani et al., 2012, Cooper and
76 Abbatt, 1996). Owing to the sufficiently high metal concentrations in tropospheric aerosols, as shown
77 in previous field measurements (Hofmann et al., 1991; Wilkinson et al., 1997; Guieu et al., 1997; Manoj
78 et al., 2000; Halstead et al., 2000; Siefert et al., 1998; Sedlak and Hoigné, 1993; Guo et al., 2014), recent
79 studies have proposed that γ may be dominated by metals contained in the aerosol. This can lead to the



80 HO₂ destruction (Mao et al., 2013a; George et al., 2013), forming H₂O₂, HO₂-water complexes, or water
81 and sulfate (Mozurkewich et al., 1987; Cooper and Abbatt, 1996; Gonzalez et al., 2010; Loukhovitskaya
82 et al., 2009; Mao et al., 2010; Macintyre and Evans, 2011), which are important in the evolution of the
83 chemical composition and physical properties of particles (George and Abbatt, 2010; George et al.,
84 2008). The available data concerning HO₂ uptake kinetics onto ambient aerosols are insufficient for
85 quantitative consideration owing to the much lower k_a value, as compared with the HO₂ reactivity of
86 ambient gases (k_g). Therefore, they are below the detection limits of the current instruments.

87 To our knowledge, aside from us, only one study has measured γ , using an offline method that
88 integrated ambient aerosols over size and time (Taketani et al., 2012). Considering that the offline
89 method may distort γ , we developed an online approach to evaluate HO₂ uptake kinetics onto ambient
90 aerosols. This method was successfully applied in Kyoto, Japan, in summer 2018, using a versatile
91 aerosol concentration enrichment system (VACES) and a technique combining laser-flash photolysis
92 with laser-induced fluorescence (LFP-LIF) (Zhou et al., 2019b). The obtained average γ value (~0.24)
93 was comparable with the previous values used for modeling studies (~0.2) (Stadtler et al., 2018; Jacob,
94 2000). However, the large standard deviation (± 0.20 , 1σ) of γ along with the measurement time suggest
95 that many other parameters might play a role, e.g., the measurement setup, aerosol characteristics, T ,
96 and RH.

97 In this study, we chose Yokohama (Japan), a coastal city with higher pollutant levels than Kyoto
98 and different properties of the air masses from mainland Japan and the coast, as the measurement site.
99 This is part of the Air QUALity Study (AQUAS) campaigns. The chemical and physical properties of
100 ambient aerosols were quantified in real-time. To test their influence on k_a and γ , we conducted
101 correlation matrix analysis coupled with the bootstrap method and classified the arriving air masses
102 from different directions. Further, the main mechanism of γ was investigated by comparing the real-
103 time quantified γ values with the modeled values. The impact of the peroxy radical's loss onto ambient
104 aerosols on air quality is evaluated through their impact on ozone formation rates and their sensitivity
105 to NO_x. The results obtained here will for better estimation of the heterogeneous reaction between HO₂
106 and ambient aerosols in sophisticated air quality models.



107 2 Materials and methods

108 2.1 Sampling sites

109 The measurement campaign was conducted at Yokohama Environmental Science Research Institute in
110 Yokohama, Japan (location: 35°28'52.8"N, 139°39'30.3"E), from July 24 to August 03, 2019. The
111 sampling ports of the instruments were placed approximately 25 m above the ground. Figure S1 shows
112 the air mass directions during the campaign, which can be classified into two categories: (i) from the
113 sea to the north, toward Yokohama City (~19% of the experimental period: from 12:00 July 25 to 12:00
114 July 27, 2019) and (ii) from the mainland toward Yokohama City (~81% of the experimental period).
115 This classification was intended to distinguish the chemical properties of aerosols arriving from the
116 mainland and the ocean, and to consequently quantify their impacts on k_a and γ .

117 2.2 Measurement strategies, instrumentation, and related data analysis

118 **LFP-LIF and VACES** In situ ambient air HO₂ reactivity was measured using LFP-LIF, which was
119 adapted from a laser-induced pump and probe OH reactivity measurement technique. This approach
120 has been successfully employed for gas and aerosol phase HO_x (=OH+HO₂) reactivity measurements
121 (Sadanaga et al., 2004; Miyazaki et al., 2013; Sakamoto et al., 2018). Further details concerning the
122 HO₂ reactivity measurements are described in the Supporting Information (SI). To compensate for the
123 relatively low ambient aerosol concentrations and thus the low k_a , a setup with VACES and an auto-
124 switching aerosol filter was used before LFP-LIF. The enrichment factor of the ambient aerosol surface
125 area (E) was calculated from the difference between the surface areas measured before and after VACES
126 by two scanning mobility particle sizers (SMPSs) (see SI).

127 HO₂ reactivities in ambient air caused by two modes were measured: (a) the gas phase mode
128 with aerosol filter on, the HO₂ reactivities are represented as k_g , and (b) the gas + enriched aerosol phase
129 mode with aerosol filter off, the HO₂ reactivities are represented as $k_g + Ek_a$, where E represents the
130 enrichment factor of k_a , Ek_a represents the total HO₂ reactivities caused by enriched ambient aerosols,
131 the usage of Ek_a is based on the assumption that HO₂ uptake with aerosol particles follows the pseudo-
132 first-order rate law. We modeled k_g in both modes using a theory identified previously (see SI: HO₂



133 reactivity of ambient gas phase) (Zhou et al., 2019b) and compared it with the measured values. The
134 differences between measured and modeled k_g in mode (a) enabled us to establish their interrelationship
135 and to check instrument stability. The differences between $(k_g + Ek_a)$ and the modeled k_g in mode (b) are
136 considered as the enriched aerosol phase HO_2 reactivity (Ek_a). The total HO_2 reactivity decay profile
137 follows single-exponential decay:

$$138 \quad \text{HO}_2 = [\text{HO}_2]_0 \exp(-(k_g + Ek_a + k_{\text{bg}})t) \quad (1)$$

139 where k_{bg} denotes the zero air background obtained by injecting zero air with the same RH as the real-
140 time ambient value into the reaction cell every 24 h for 30 min. The RH was controlled by passing some
141 of the zero air through a water bubbler. The value of k_{bg} was subtracted separately on each day. The
142 variability of k_{bg} (i.e., the reproducibility of the laser system) was calculated as the standard deviation
143 of the response of repeated measurements on different days. It was found to be $\sim 4\%$, which is slightly
144 higher than the instrument precision (3%). A 30-min average calculation was applied to the data to
145 reduce data fluctuation. The observed HO_2 uptake coefficients onto ambient aerosols (γ_{obs}) can be
146 calculated from the dependence of Ek_a on γ_{obs} :

$$147 \quad Ek_a = \frac{\gamma_{\text{obs}} \omega_{\text{HO}_2} ES}{4} \quad (2)$$

148 where ES and ω_{HO_2} represent the enriched surface area of ambient aerosol after VACES (~ 12.5) and
149 the mean thermal velocity of HO_2 ($\sim 437.4 \text{ m s}^{-1}$), respectively. Therefore, the HO_2 reactivity of ambient
150 aerosol (k_a) can be obtained from Ek_a by dividing by the enrichment factor E .

151 **High resolution–time of flight–aerosol mass spectrometry (HR–ToF–AMS)** A field-deployable HR–
152 ToF–AMS (Aerodyne Research Inc.) (DeCarlo et al., 2006) was used for the characterization of the
153 non-refractory aerosol mass with a time resolution of ~ 3 min. The HR–ToF–AMS measured the total
154 organic aerosol (OA), sulfate (SO_4^{2-}), nitrate (NO_3^-), ammonium (NH_4^+), chloride (Cl^-), and the two
155 most dominant oxygen-containing ions in the OA spectra, i.e., mass-to-charge ratios of $m/z = 44$ (Org44,
156 mostly CO_2^+) and $m/z = 43$ (Org43, mainly $\text{C}_2\text{H}_3\text{O}^+$ for the oxygenated OA and C_3H_7^+ for the
157 hydrocarbon-like OA) (Ng et al., 2011). The fractions of Org44 and Org43 in OA are represented as f_{44}
158 and f_{43} , respectively. Ambient air was sampled through a critical orifice into an aerodynamic lens, which



159 efficiently transmitted particles between 80 nm and up to at least 1 μm . Particles were flash-vaporized
160 by impaction on a resistively heated surface (~ 600 °C) and ionized by electron ionization (70 eV). The
161 m/z values of the resulting fragments were determined using a ToF mass spectrometer. Data were
162 analyzed using the ToF-AMS software SQUIRREL and PIKA. Data were not corrected for lens
163 transmission efficiency. Standard relative ionization efficiencies (RIE) were used for organics (RIE =
164 1.4), nitrate (RIE = 1.1), chloride (RIE = 1.3), sulfate (RIE = 1.12), and ammonium (RIE = 4).
165 Concentration data were obtained from background-subtracted stick-mass data (low-mass-resolution-
166 base mass concentration data, which are calibrated using ammonium sulfate particles) and determined
167 assuming a collection efficiency (CE) of 0.5.

168 **Filter-based photometer** Real-time measurement of the equivalent black carbon (eBC) was performed
169 using a 5-wavelength dual-spot absorption photometer (MA300, AethLabs, San Francisco, CA, USA),
170 which performed an online correction for possible artefacts resulting from filter loading and multiple
171 scattering (Drinovec et al., 2015). In this study, eBC data obtained from light attenuation at a wavelength
172 of 880 nm were used to avoid possible contributions from brown carbon; the time resolution was ~ 1
173 min.

174 **Trace elements** Fourteen trace elements (Al, V, Cr, Mn, Co, Ni, Cu, Zn, As, Se, Sr, Cd, Ba, and Pb)
175 were measured using an offline method at two-day intervals from 21 July to 5 August 2019. The
176 suspended particle matter (SPM) was collected onto 623.7 cm^2 size quartz fiber filters (Pallflex
177 Tissuquartz 2500QAT-UP), which had an available collecting area of 405.84 cm^2 , using a high-volume
178 sampler (1000 L min^{-1}). Approximately 2 cm^2 of each filter was cut into pieces and placed into a
179 polytetrafluoroethylene (PTFE) pressure digestion tank with 1 mL 49% hydrofluoric acid (HF) and 5
180 mL 69% nitric acid (HNO_3). A Thermo Fisher X2 Series inductively coupled plasma mass spectrometer
181 (ICP-MS) was then used to determine metal concentrations. By assuming that the metal fractions were
182 the same in SPM and PM_{10} (aerosol particles with aero-dynamic diameters less than 1 μm), the
183 concentrations in PM_{10} were estimated according to the tested metal concentrations in SPM and the ratio
184 between SPM and PM_{10} measured in-situ.



185 **Water-soluble inorganic species** NR-PM₁ water-soluble inorganic species (including Na⁺, SO₄²⁻, NH₄⁺,
186 NO₃⁻, Cl⁻, Ca²⁺, K⁺, Mg²⁺) used for the *ISORROPIA-II* model were also measured using offline method,
187 as described above. For extraction, we cut 1/4 of a 47 mm filter punched from the original collected
188 filter and placed it in 10 mL of ultrapure water (18.2 MW cm⁻¹) in a centrifuge tube. This was followed
189 by 15 min of ultrasonication in a 30°C water bath. The solution was then vortexed (Vortex Genie 2,
190 Scientific Industries, USA) for 1 min to ensure homogeneity and filtered through syringe filter with
191 pore size of 0.45-µm (Advantec Dismic-25, PTFE). An Ion Chromatograph (IC, ICS1600, DIONEX,
192 USA) was employed to determine the concentrations of these inorganic ions in the extracted solution.

193 **Scanning Mobility Particle Sizers (SMPS)** Particle mass and surface area before and after VACES
194 were determined using two SMPSs (model 3936L72 and 3936L75, TSI, Shoreview, MN, USA) that
195 measured particle size distribution at 14.1–736.5 nm and 14.6–661.2 nm at 5-min intervals.

196 **Gas phase monitors** NO₂ was measured by cavity attenuated phase shift (CAPS, Aerodyne Research,
197 USA, at 1-s intervals), NO_y–NO by chemiluminescence (Model 42i-TL, Thermo, at 10-s intervals),
198 CO by Thermo CO analyzer of nondispersive infrared spectroscopy (Model 48i-TLE, Thermo Scientific,
199 USA, at 10-s time intervals), and O₃ by UV absorption (Model 1150, Dylec, AMI Co., Ltd, at 10-s time
200 intervals). HCHO was determined by high performance liquid chromatography (HPLC; 1260 Infinity,
201 Agilent Technologies Inc, USA) from 14:00 July 29, to 12:00 August 3, 2019. An average value of ~2
202 ppb was used for the data analysis.

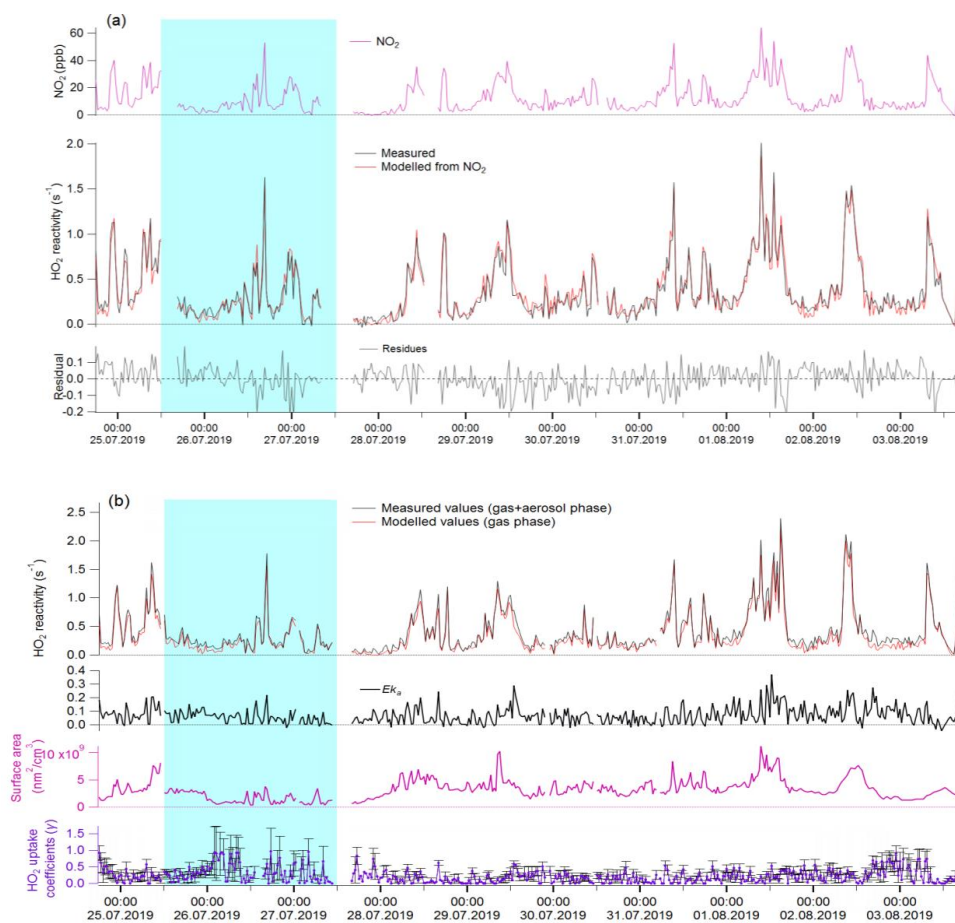
203 **ISORROPIA-II model** NR-PM₁ water-soluble inorganic species (including Na⁺, SO₄²⁻, NH₄⁺, NO₃⁻, Cl
204 ⁻, Ca²⁺, K⁺, Mg²⁺) and meteorological parameters including temperature and RH were used to calculate
205 the aerosol pH and liquid water content based on the *ISORROPIA-II* model (Fountoukis and Nenes,
206 2007). We ran *ISORROPIA-II* in “reverse” mode and the particles were assumed to be deliquescent, i.e.,
207 in metastable mode (Hennigan et al., 2015). The thermodynamic equilibrium of the NH₄⁺- SO₄²⁻- NO₃
208 ⁻ system case was used for modeling.

209 3 Results and discussion

210 3.1 The HO₂ uptake kinetics onto ambient aerosols



211 The measured total HO₂ reactivities were compared against the modeled gas phase HO₂ reactivity under
212 the experimental conditions both with and without the aerosol phase. Without the aerosol phase, the
213 modeled k_g values are calculated according to the description in Sect. 2.2, which are not statistically
214 different with the measured k_g values (Fig. 1a second panel, T-test, $p = 0.49$, with $\alpha = 0.05$),
215 indicating that HO₂ loss in the reaction cell was dominated by its reaction with NO₂ in the LFP-LIF
216 system. With the aerosol phase, the measured ($Ek_a + E_g$) and modeled values ($\approx E_g$) were significantly
217 different (see Fig. 2b, first panel, T-test, $p = 0.04$, with $\alpha = 0.05$). The differences were considered
218 to be the HO₂ reactivities of enriched ambient aerosols (Ek_a). Ek_a ranged between 0.01 s^{-1} (25th percentile)
219 and 0.1 s^{-1} (75th percentile), with an average value of $0.066 \pm 0.062 \text{ s}^{-1}$, the corresponding k_a , calculated
220 by dividing Ek_a by E , ranged between 0.001 s^{-1} (25th percentile) and 0.08 s^{-1} (75th percentile), with an
221 average value of $0.005 \pm 0.005 \text{ s}^{-1}$. The error for Ek_a was estimated as $\sim 0.05 \text{ s}^{-1}$, calculated as the
222 propagated errors from $k_g + Ek_a$ (equals to the systematic error of the instrument, $\sim 0.05 \text{ s}^{-1}$) and the
223 modelled k_g in mode (b) ($\sim 0.001 \text{ s}^{-1}$). Accordingly, the errors for k_a was estimated as $\sim 0.004 \text{ s}^{-1}$ (from
224 the obtained error of Ek_a by dividing by the enrichment factor E). The corresponding γ , calculated
225 from Eq. 2, ranged from 0.05 (25th percentile) to 0.33 (75th percentile), with an average value of $0.23 \pm$
226 0.22. The gas-phase diffusion effects on γ were estimated to be less than 1% (i.e., negligible) (further
227 details are given in the SI).



228

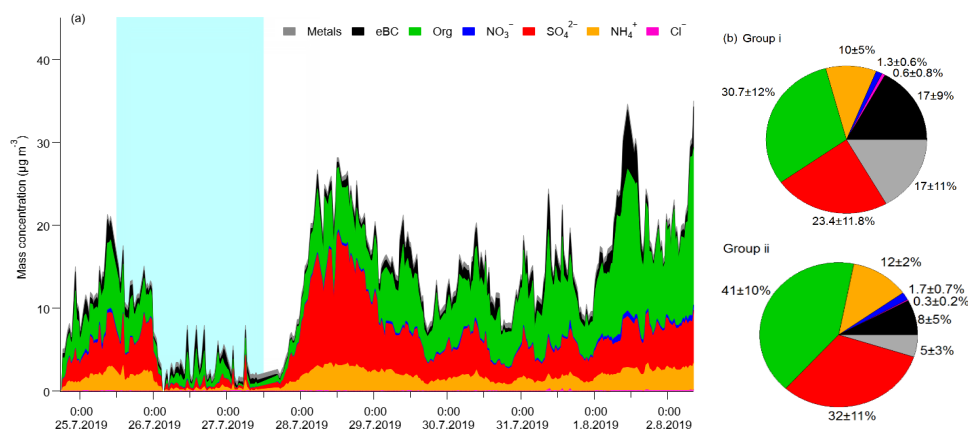
229 Figure 1: Temporal variation of parameters under different experimental conditions. (a) Without aerosol phase:
230 1st panel: measured NO₂ concentrations (ppb); 2nd panel: measured (red line) and modeled (black line) k_g ; 3rd panel:
231 fitting residues of modeled k_g values, ranging from -0.04 (25 percentile) to 0.05 (75 percentile), which are
232 considered to be the systematic error of the LFP–LIF instrument. (b) Gas + aerosol phase: 1st panel: measured
233 total HO₂ reactivity (k_g+Ek_a) and modeled k_g ; 2nd panel: Ek_a , calculated from the difference between the measured
234 and modeled values from the 1st panel; 3rd panel: the surface area of the enriched ambient aerosols (ES); 4th panel:
235 γ calculated from Ek_a and ES according to Eq. 2. The blue shaded area represents the air masses from group i
236 (from coast), the remainder is from group ii (from mainland). The errors for γ were estimated as the propagated
237 errors of k_a (~ 0.004 s⁻¹) and the surface area ($\sim 8\%$), based on the systematic errors of the instrument.

238
239 Statistical significance analysis showed that the average γ value of group i (0.35 ± 0.28) is significantly
240 higher than that of group ii (0.21 ± 0.16) (calculated $p = 4.9E-5$; Mann-Whitney), indicating that the air
241 masses from the ocean yield higher γ values than the air masses from mainland Japan. This difference
242 maybe influenced by many factors, for example, the mass accommodation coefficients (α^{HO_2}), which
243 are driven by the physical and chemical properties of the aerosols. Studies have shown that α^{HO_2} are



244 typically ~ 0.2 and 0.5 for organics and inorganics, respectively (Lakey et al., 2016b, 2016a; Taketani
245 et al., 2008, 2009; Thornton et al., 2005; Moon et al., 2018; George et al., 2013; Mozurkewich et al.,
246 1987), while for aerosols with transition metals, γ values could be limited only by α^{HO_2} (Mozurkewich
247 et al., 1987). Thus we will discuss such differences in the aerosols arriving from the ocean (group i) and
248 the mainland (group ii) in the following sections (more details can be found in Sect. 3.4 and Table S1).
249 The average value of k_a at Yokohama ($0.005 \pm 0.005 \text{ s}^{-1}$) was much higher than that found for Kyoto
250 city ($0.0017 \pm 0.0015 \text{ s}^{-1}$) (with calculated $p < 0.05$; Mann-Whitney), this may due to many differences
251 in aerosol properties in Kyoto and Yokohama city. We list some of them as follows: 1) mass
252 composition, the aerosols in the coast city tend to contain more sea salts thus increased k_a , 2) particle
253 size distribution, smaller particles tending to yield higher γ values than larger particles owing to the
254 limitation of gas phase diffusion is smaller with micrometer particles, and the distribution of depleting
255 species (e.g., transition metal ions) are mostly distributed in accumulation mode of aerosol, 3) the water
256 content and the metal concentrations, this will highly influence the HO_2 uptake capacity of the ambient
257 aerosols. However, the average HO_2 uptake coefficient onto ambient aerosols (γ) in Yokohama (~ 0.23)
258 was comparable with previous measured ($\sim 0.24\text{--}0.25$) (Zhou et al., 2019b; Taketani et al., 2012) and
259 modeled (~ 0.20) values (Stadtler et al., 2018; Jacob, 2000). The large standard deviation (± 0.21 , 1σ)
260 of the values along with the measurement time may be due to the instantaneously changed chemical
261 and physical properties of ambient aerosols, indicating that a large bias may exist if a constant γ value
262 is used for modeling.

263 3.2 Bulk chemical composition of ambient aerosols



264

265 Figure 2: (a) Concentrations of non-refractory chemical components plus eBC in Yokohama, Japan (July 24 to
266 August 02, 2019). The blue shaded area represents group i from coast and the remaining areas represent group ii
267 from mainland. (b) Average contribution fractions of different chemical components of groups i and ii.
268

269 Figure 2a shows the time series of the mass concentrations of OA, SO_4^{2-} , NO_3^- , NH_4^+ , Cl^- , and eBC in
270 PM_1 in Yokohama from July 24 to August 02, 2019, which is ~ 1.5 days less than for the LFP–LIF data.
271 During this period, PM_1 ranged from ~ 1 to $35 \mu\text{g m}^{-3}$ (average $\approx 13 \mu\text{g m}^{-3}$) and was dominated by OA,
272 SO_4^{2-} , and NH_4^+ , with contributions of $39 \pm 11\%$, $30 \pm 12\%$, and $12 \pm 4\%$, respectively; these were
273 followed by eBC and metals, with contributions of $10 \pm 7\%$ and $8 \pm 8\%$, respectively. Cl^- contributed
274 $< 1\%$ in both groups, which is similar to that reported for an urban area in winter in Bern (Switzerland)
275 (Zhou et al., 2019a). However, NO_3^- contributed much less ($\sim 2 \pm 0.7\%$) compared with that reported
276 for Bern ($\sim 19 \pm 4\%$), which may be due to the reverse reaction of NH_4NO_3 converting to HNO_3 . Since
277 Yokohama is a coastal city, and HNO_3 is easy vaporized in summer, gaseous HNO_3 may sink with sea
278 salt particles by forming NaNO_3 through heterogeneous reactions (Finlayson-Pitts and Pitts, 2000).

279 Figure 2b shows the average contribution fractions of different components of group i and group
280 ii. The main differences in the components between these two groups are the fractions of OA, BC, SO_4^{2-} ,
281 and metals. The OA fraction was ~ 1.8 and ~ 8.4 times higher than that for the metals in groups i and ii,
282 respectively. As OA can cover the surface of the particles and thereby decrease γ (Lakey et al., 2016a;
283 Takami et al., 2013), the difference between the OA and metal fractions in these two groups may
284 partially explain the much higher γ values of group i (vs. group ii). Previous studies have shown quite



285 low HO₂ uptake coefficient on BC (~ 0.01) (Saathoff et al., 2001; Macintyre and Evans, 2011), which
286 in contrast to the results obtained here. This may due to the much higher fraction of eBC in group i
287 (vs. group ii) may also provide active sites thus facilitating the physical uptake of HO₂. We also
288 observed slightly higher Cl⁻ and BC fraction in group i (from ocean) than that of group ii (from
289 mainland), which may due to the effects of sea salt and the ship emissions, respectively. From the
290 average diurnal patterns (Figs. S5 and S6), the trends in k_a follow the trends in chemical composition,
291 whereas γ shows a contrasting trend with both variables in both groups. For group ii, SO₄²⁻ and OA
292 exhibited higher values whereas γ exhibited lower values during the daytime than those during nighttime,
293 indicating that secondary aerosol formation resulting from photochemical reactions may decrease γ . To
294 identify the influence of each individual chemical component of ambient aerosol on k_a and γ , we further
295 performed correlation matrix analysis.

296 **3.3 Influence of individual chemical components of ambient aerosol on k_a and γ**

297 For the ambient aerosol with multiple components, k_a and are influenced by many factors, and those
298 factors also have mutual effects to each other, for example, the transition metal Cu and Fe contained in
299 ambient aerosols can be chelated by organics (Lakey et al., 2016b). The direct correlations between
300 transition metals and γ may give us some hints about the interactions of different chemical components
301 in ambient aerosols and their effects to γ . Therefore, we produced a Pearson correlation matrix of all
302 the testing chemical composition factors in Yokohama city. To exclude the effects of the different
303 fractions of chemical components in groups i and ii, the bootstrap method, which is based on the creation
304 of replicate the inputs by perturbing the original data through resampling, was employed. The
305 resampling was performed by randomly reorganizing the rows of the original time series such that some
306 rows of the original data were present several times while other rows were removed. The final results
307 were obtained by running the data for 1000 bootstrap replicates. The average values of these 1000
308 bootstrap replicates are listed in Fig. 3.



309

310 Figure 3: Correlation matrix showing Pearson's r values for the chemical compositions, k_a , and γ during the
 311 corresponding measurement periods (in the blue box), as well as the Pearson's r values for the chemical
 312 composition fraction i (represented as f_i , $i = OA, SO_4^{2-}, NH_4^+, NO_3^-, Cl^-, eBC$, and metals) and γ (in the dashed
 313 line box).

314

315 Most of the chemical components had strong or moderate Pearson correlation coefficients with each

316 other (Fig. 3), although k_a and γ showed only a moderate correlation with each other (0.56). As γ can be

317 correlated with the qualitative, rather than quantitative, properties of the aerosols, we further

318 investigated the Pearson's r values between the chemical composition fractions and γ . The results show

319 that k_a was positively correlated with total mass and the individual chemical components, whereas γ

320 showed only a weak positive correlation with f_{metals} (0.30) and f_{eBC} (0.18). This indicates that the

321 metals may act as a catalyst, thus accelerating the depletion of HO_2 (Mao et al., 2013a) (chemical

322 reaction), and that BC may provide the active sites for HO_2 radical interaction with ambient aerosols

323 (physical uptake). The very weak correlation of γ with f_{Cl^-} (0.04) may be related to Cl^- chemistry, for

324 example, $HO_2(g)$ can react with $NaCl(g)$ and produce $NaOH$ and $Cl_2(g)$, thus cause a decrease in the

325 HO_2 concentration, which in turn indirectly effects γ (Remorov et al., 2002). Interestingly, when

326 considering the Org₄₄ and Org₄₃ fractions in total OA separately, γ is positively correlated with f_{43}

327 (0.18) but negatively correlated with f_{44} (-0.24). This is consistent with the conclusion from Lakey et

328 al. (2016b), i.e., that more oxidized organic aerosols tend to be highly viscous and thus decrease HO_2

329 uptake coefficients (Lakey et al., 2016b). In summary, γ was dominated by the free forms of transition



330 metals that can act as catalysts of HO₂ uptake onto ambient aerosols, and was indirectly affected by
331 chemical components that might alter the properties of ambient aerosols, e.g., oxygenated OA can cover
332 the aerosol surface and alter the viscosity of ambient aerosols, thereby decreasing γ (Lakey et al., 2016a;
333 Lakey et al., 2016b; Takami et al., 2013), whereas BC may provide active sites and thereby increase γ
334 though physical uptake. This is further confirmed by the classification of the air masses, i.e., the air
335 mass from the ocean (group i), which had a higher HO₂ uptake capacity, contained less OA and more
336 metals than that from mainland Japan (group ii). We further compared the measured γ values with the
337 modeled γ values using previously proposed mechanisms, as shown below.

338 **3.4 Possible mechanism of HO₂ uptake onto ambient aerosols**

339 Two mechanisms of HO₂ uptake onto aqueous ambient aerosols have been proposed, for which
340 equations have been derived from a previous study (Thornton et al., 2008): (i) HO₂-only chemistry and
341 (ii) chemistry with transition metals playing a role. In this study, the liquid content of the total ambient
342 aerosol mass ranged from 70% to 88%, as obtained from the *ISORROPIA-II model*. As the solubility of
343 Fe is rather small in ambient aerosol, the reaction rates of Fe/Mn for liquid phase HO₂ in aerosol is ~
344 100 times slower than it is for Cu, thus the influence of Fe and Mn on HO₂ uptake can be neglected
345 compared to Cu or scaled as equivalent [Cu²⁺] (Fang et al., 2017; Hsu et al., 2010; Baker and Jickells,
346 2006; Oakes et al., 2012; Song et al., 2020), therefore, we use the soluble Cu as surrogate for transition
347 metals in ambient aerosols to assess the influence of transition metals to γ in ambient aerosols. The Cu
348 solute mass fraction in the liquid content of the ambient aerosols was estimated as $(3.5\text{--}30) \times 10^{-4}$ mol
349 L⁻¹ according to our offline filter test (Sect. 2.2), and the activity coefficient for total Cu was assumed
350 to be 0.1 (upper limit) based on a study of (NH₄)₂SO₄ particles at 68% RH (Ross and Noone, 1991).
351 Using copper ions as a surrogate metal for transition metal ions (TMIs), the potential HO₂ loss onto
352 aqueous ambient aerosols via mechanisms involving TMIs was estimated as (Hanson et al., 1994):

$$353 \frac{1}{\gamma^{\text{TMI}}} = \frac{1}{\alpha^{\text{HO}_2}} + \frac{\omega}{H_{\text{eff}} RT \sqrt{k^{\text{I}} D_{\text{aq}} Q^{\text{I}}}} \quad (3)$$

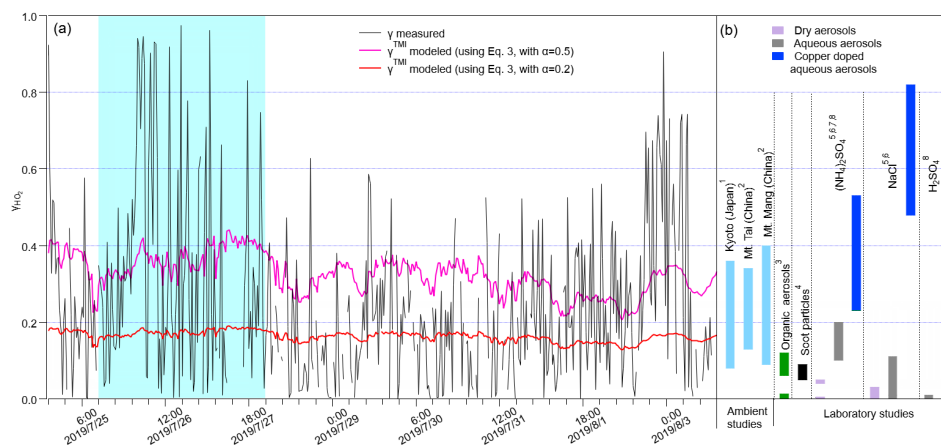
354 where α^{HO_2} is the mass accommodation coefficient of HO₂, ω is the mean HO₂ molecular speed (cm s⁻¹),
355 H_{eff} is the effective Henry's Law coefficient, R is the gas constant (J K⁻¹ mol⁻¹), and T the temperature



356 (K). k^I is the pseudo-first-order rate constant equal to $k_{\text{TMI}}^{\text{H}}[\text{TMI}]$, where $k_{\text{TMI}}^{\text{H}}$ is the second order rate
357 constant for aqueous phase reaction with HO_2/O_2^- and TMI. Q' accounts for aqueous-phase diffusion
358 limitations and is expressed as

$$359 \quad Q' = [\coth(q) - \frac{1}{q}]; \quad q = r_p \sqrt{\frac{k^I}{D_{aq}}} \quad (4)$$

360 Table S1 shows more details of the parameters used for modeling. γ^{TMI} with $\alpha^{\text{HO}_2}=0.2$ (typically for
361 organics) and 0.5 (typically for inorganics as explained in Table S1) are plotted in Fig. 4a along with the
362 measured γ values; the much lower variation of the modeled values may due to the low time resolution (~ 2
363 days) of [Cu]. The measured γ values (averaged value: ~ 0.23) are significantly lower than the modelled
364 γ^{TMI} with $\alpha^{\text{HO}_2}=0.5$ (averaged value: ~ 0.32), but significantly higher than the modelled γ^{TMI} with
365 $\alpha^{\text{HO}_2}=0.2$ (averaged value: ~ 0.16), both with calculated $p < 0.05$ (t-test), indicating that the chemical
366 components may be internally mixed, as proposed by Takami et al. (2013), which influences the aerosol
367 surface tension and the activity of the free form of the copper ion (i.e., OA and BC) to constrain γ^{TMI} ;
368 however, this is not considered in this model. No linear correlation was found between γ^{TMI} and γ . Further
369 classification of measured $\gamma \geq 0.4$ and $\gamma < 0.4$ shows that γ^{TMI} has a weak correlation with measured γ values
370 when $\gamma \geq 0.4$ (Fig. S7), which may due to the higher fraction of metals in the total mass at measured $\gamma \geq 0.4$
371 ($\sim 12\%$) than at < 0.4 ($\sim 7\%$); therefore, the impact of the other chemical components is much lower. The γ
372 values obtained here are comparable with those in previous ambient aerosol studies (Taketani et al., 2008;
373 Zhou et al., 2019b) (Fig. 5b). When compare with single-compound aerosols obtained from laboratory
374 studies, γ values were generally higher than the HO_2 uptake coefficients onto organic species (Lakey et al.,
375 2015), soot particles (Bedjanian et al., 2005), and the dry state of inorganic aerosols (i.e., $(\text{NH}_4)_2\text{SO}_4$, NaCl,
376 and H_2SO_4), but comparable or lower than aqueous and copper-doped aqueous phases of inorganic species
377 (Fig. 5b) (George et al., 2013; Lakey et al., 2016b; Taketani et al., 2008; Thornton and Abbatt, 2005). This
378 may indicate the collective effects of the individual chemical components of ambient aerosols to γ , and the
379 significant influence of RH to aerosol states of single-component particles thus their HO_2 uptake coefficients.



380

381 Figure 4: (a) Measured and modeled γ values along with measurement time. The blue shaded area represents group
382 i; the remaining areas represent group ii. (b) HO_2 uptake coefficients onto different types of aerosol obtained from
383 ambient and laboratory studies, the numbers indicate the related references from which the data were obtained: 1.
384 Zhou et al., 2019b; 2. Taketani et al., 2012; 3. Lakey et al., 2015; 4. Bedjanian et al., 2005; 5. Taketani et al., 2008;
385 6. George et al., 2013; 7. Lakey et al., 2016b; 8. Thornton and Abbatt, 2005.

386

387 Other studies have shown that γ is strongly negatively temperature dependent (Remorov et al., 2002;

388 Mao et al., 2010; Cooper and Abbatt, 1996; Hanson et al., 1992; Thornton and Abbatt, 2005;

389 Gershenson et al., 1995). Here, RH and T were stabilized by the VACES–LFP–LIF system, as compared

390 with those in ambient air (Fig. S8). We noticed that k_a and γ showed no dependence on RH and T in the

391 reaction cell (see Fig. S9), indicating that the instantaneous change of RH and T may not be dominating

392 factors in terms of the variation of k_a and γ with measurement time. This suggests that the individual

393 chemical components and physical properties of ambient aerosols may dominate γ variation during field

394 campaign; both the metal-catalyzed reactions and the chemical components and their states should be

395 considered to yield more accurate γ values. Results obtained here are in accordance with previous results

396 on correlations between particulate H_2O_2 (which can be formed by the uptake of HO_2) and coarse

397 particulate transition metals (Wang et al., 2010). Using an offline methodology to investigate the

398 influence of RH and T by maintaining constant experimental conditions or chemical compositions will

399 be the subject of future work.

400 3.5 Influence of the physical properties of ambient aerosols on k_a and γ

401 HO_2 heterogeneous loss rates are driven by the different particle sizes of different aerosol types (i.e.,

402 urban ambient aerosols and marine aerosols)(Morita et al., 2004; Guo et al., 2019; Jacob, 2000). In this



403 study, k_a and γ showed no linear dependence on the mean ambient particle diameters (see Fig. S10).
404 Identifying the fractional contributions of aerosols in different particle size ranges to k_a and γ is highly
405 desirable in terms of understanding their influence. However, it seems that high γ values (> 0.8) occur
406 when the surface area is $< 2 \times 10^{-6} \text{ cm}^2 \text{ cm}^{-3}$ and the mean particle diameter is $< 110 \text{ nm}$. This is in
407 accordance with a previous study showing that aerosols yield the highest fractional contribution to the
408 total heterogeneous loss rate of HO_2 radicals of size $< 0.1 \mu\text{m}$ (Morita et al., 2004) and that the mass
409 accommodation process plays the determining role for small and medium sized aerosols in controlling
410 HO_2 uptake. Guo et al. (2019) states the HO_2 radicals experience less loss upon diffusion onto large
411 aerosols than do small droplets due to dilution effects make the larger aerosols having lower depleting
412 species concentrations (Cu^{2+}). However, this was based on the assumption that the total mass of Cu^{2+} is
413 constant during the hygroscopic growth of particles which is not always true in the ambient conditions.
414 Further studies about Cu^{2+} content in particles with different size distribution are needed to fully
415 understand the result here.

416 3.6 Significance of k_a to O_3 formation potential

417 In urban atmosphere, XO_2 ($=\text{HO}_2+\text{RO}_2$) fate is important to the photochemical production of ozone
418 ($\text{P}(\text{O}_3)$). Here, the loss rates of XO_2 due to three factors were compared: (i) uptake onto the ambient
419 aerosols ($L_{\text{P-XO}_2}$ in Eq. 5), since no experiment or reference available for RO_2 uptake onto ambient
420 particles, we assume the RO_2 reactivities caused by its interaction with ambient aerosols were the same
421 as k_a , (ii) XO_2 self-reactions ($L_{\text{R-XO}_2}$ in Eq. 6), and (iii) reaction with NO ($L_{\text{N-XO}_2}$ in Eq. 7), which can
422 produce NO_2 , a precursor of O_3 ; therefore Eq. 7 can also be regarded as $\text{P}(\text{O}_3)$.

$$423 L_{\text{P-XO}_2} = k_a[\text{XO}_2] \quad (5)$$

$$424 L_{\text{R-XO}_2} = 2 * (k_{\text{HO}_2-\text{HO}_2}[\text{HO}_2]^2 + k_{\text{HO}_2-\text{RO}_2}[\text{HO}_2][\text{RO}_2]) \quad (6)$$

$$425 L_{\text{NO-XO}_2} = k_{\text{NO-XO}_2}[\text{NO}][\text{XO}_2] = \text{P}(\text{O}_3) \quad (7)$$

426 where $k_{\text{HO}_2-\text{HO}_2}$ and $k_{\text{HO}_2-\text{RO}_2}$ are the second-order rate constants of HO_2 self-reaction and its reaction
427 with RO_2 , respectively. $k_{\text{NO-HO}_2}$ is the second-order rate constant of the reaction of HO_2 with NO . The
428 HO_2 concentration was estimated from O_3 concentration using the method described by Kanaya et al.,



429 (2007a). The RO₂ concentration is then estimated by assuming a steady state of HO₂ in the HO_x cycle;
 430 the reaction rates of HO₂ radicals are approximated as 0:

$$431 \frac{d[\text{HO}_2]}{dt} = P_{\text{HO}_2} - L_{\text{HO}_2} = k_{\text{CO-OH}}[\text{OH}][\text{CO}] + k_{\text{H}_2\text{CO-OH}}[\text{OH}][\text{H}_2\text{CO}] + k_{\text{NO-RO}_2}[\text{RO}_2][\text{NO}] -$$

$$432 2k_{\text{HO}_2\text{-HO}_2}[\text{HO}_2][\text{HO}_2] - k_{\text{HO}_2\text{-RO}_2}[\text{HO}_2][\text{RO}_2] - k_{\text{NO-HO}_2}[\text{HO}_2][\text{NO}] - ka[\text{HO}_2] = 0 \quad (8)$$

433 where $k_{\text{CO-OH}}$ and $k_{\text{H}_2\text{CO-OH}}$ are the second-order rate constants of the reactions of CO and H₂CO with
 434 OH, respectively. The different XO₂ loss rates described in Eqs. 5–7, along with the measurement times,
 435 are shown in Fig. 5a. Generally, $L_{\text{P-XO}_2}$ is much greater than $L_{\text{R-XO}_2}$, indicating that the XO₂ taken up
 436 by ambient aerosols will compete with the XO₂ self-reaction, thus influencing XO₂ concentration.
 437 However, such an influence may have a negligible impact on P(O₃) because $L_{\text{P-XO}_2}$ is tens of thousands
 438 times lower than $L_{\text{NO-XO}_2}$ owing to the relatively high NO_x concentration in Yokohama. We further
 439 tested the impact of $L_{\text{P-XO}_2}$ on ozone formation sensitivity regime, according to the method proposed
 440 by Sakamoto et al. (2019), in which L_{N}/Q is used as a new indicator:

$$441 \frac{L_{\text{N}}}{Q} = \frac{1}{1 + \frac{(2k_{\text{R}}[\text{XO}_2] + k_{\text{a}}')k_{\text{OH-VOCs}}[\text{VOCs}]}{(1-\alpha')k_{\text{NO-HO}_2}[\text{NO}]k_{\text{OH-NO}_2}[\text{NO}_2]}} \quad (9)$$

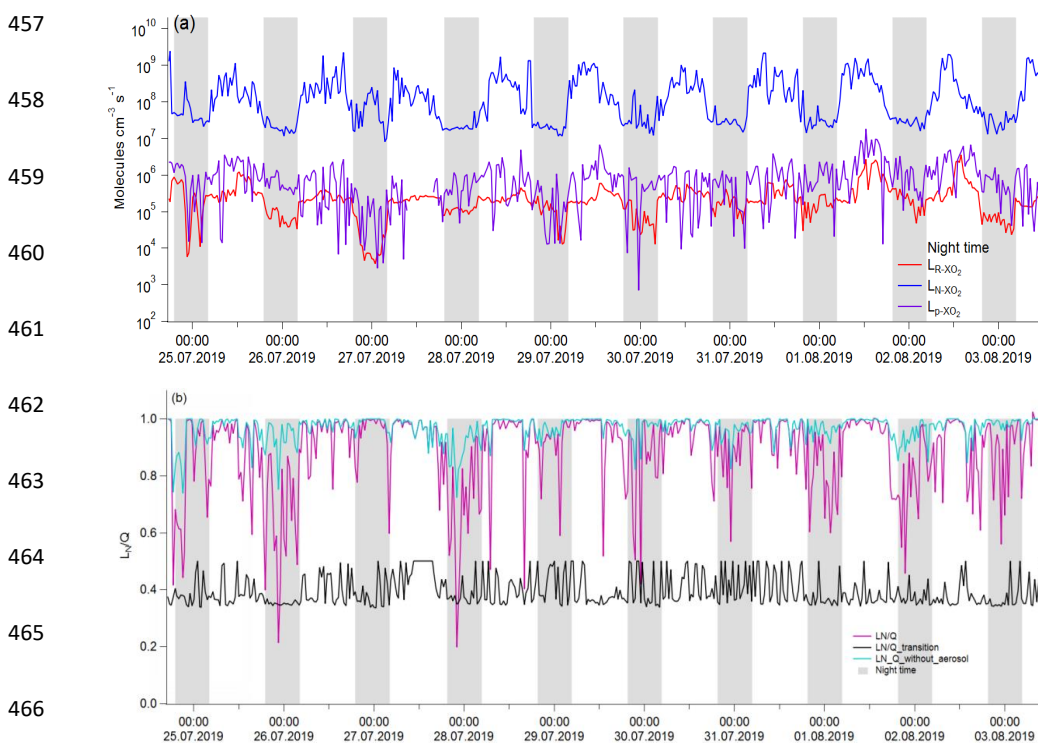
442 where $k_{\text{OH-VOCs}}$ and $k_{\text{OH-NO}_2}$ are the second-order rate constants of the reactions of OH with VOCs
 443 and NO₂, respectively. $k_{\text{NO-HO}_2}$ is the second-order rate constant of the reaction of NO with HO₂. α'
 444 is the proportion of RO₂ in XO₂. L_{N} is the OH radical loss rate through its reaction with NO₂. (= $k_{\text{OH-NO}_2}[\text{OH}][\text{NO}_2]$), and Q is the total loss of the HO_x radicals in the HO_x cycle reaction (= $L_{\text{N}} +$
 445 $L_{\text{P-XO}_2} + L_{\text{R-XO}_2}$). The regime transition point can be expressed as

$$447 \frac{L_{\text{N}}}{Q_{\text{transition}}} = (1 - \chi)\frac{1}{2} + \chi\frac{1}{3} \quad (10)$$

448 where $\chi = L_{\text{P-XO}_2} / (L_{\text{P-XO}_2} + L_{\text{R-XO}_2})$. The results indicate that both L_{N}/Q and $L_{\text{N}}/Q_{\text{without_aerosol}}$
 449 (calculated with and without including k_{a}' in Eq. 9, respectively) were higher than $L_{\text{N}}/Q_{\text{transition}}$,
 450 indicating that ozone formation was VOC-sensitive throughout the campaign and that the aerosol uptake
 451 of XO₂ (k_{a}') showed no impact on the O₃ formation regime (see Fig. 5, here we only consider the
 452 daytime, when photochemical reactions occur). The plots of L_{N}/Q and $L_{\text{N}}/Q_{\text{without_aerosol}}$ as a



453 function of NO concentration show the values were closer to $L_N/Q_{\text{transition}}$ (~ 0.4) at lower NO
454 concentrations (Fig. S11); therefore, aerosol uptake may play a more important role in the O_3 formation
455 regime at NO levels lower than those observed in this study. The temporal variations in key factors used
456 in this section are shown in Fig. S12.



467 Figure 5: Temporal variations in (a) HO_2 radical loss rates and (b) L_N/Q (red line) and the regime
468 transition threshold ($L_N/Q_{\text{transition}}$, black line) used to assess the ozone sensitivity regime. The gray
469 shaded areas represent nighttime (from National Astronomical Observatory of Japan) and are not
470 discussed herein.
471

472 4 Conclusions

473 This study used a reliable online methodology to investigate HO_2 uptake kinetics onto in situ ambient
474 aerosols (i.e., HO_2 reactivity of ambient aerosols k_a and HO_2 uptake coefficients γ) and discussed the
475 impacting factors on such processes, i.e., chemical compositions and physical properties of ambient
476 aerosols and experimental conditions. k_a ranged between 0.001 s^{-1} (25th percentile) and 0.005 s^{-1} (75th
477 percentile), with an average value of $0.005 \pm 0.005 \text{ s}^{-1}$. The corresponding γ , ranged from 0.05 (25th



478 percentile) to 0.33 (75th percentile), with an average value of 0.23 ± 0.22 , is comparable with previous
479 measured ($\sim 0.24\text{--}0.25$) (Zhou et al., 2019b; Taketani et al., 2012) and modeled (~ 0.20) values (Stadtler
480 et al., 2018; Jacob, 2000). We noticed that k_a and γ showed no dependence on RH and T in the reaction
481 cell in this study, indicating that the instantaneous change of RH and T may not be dominating factors
482 in terms of the variation of k_a and γ with measurement time, and the large standard deviation of the γ
483 values along with the measurement time (± 0.21 , 1σ) may be due to the instantaneously changed
484 chemical and physical properties of ambient aerosols, a large bias may exist if a constant γ value is used
485 for modeling.

486 We found that the individual chemical components of ambient aerosols may have collective effects
487 of to γ , through the analyses of 1) separating the air masses into two groups, group i from the ocean and
488 group ii from mainland Japan; 2) the average diurnal patterns; 3) the correlation matrix analysis of each
489 individual chemical component of ambient aerosol with γ ; and 4) the modeling studies using previously
490 proposed mechanisms. All these effects clearly indicating that the transition metals contained in ambient
491 aerosols may act as a catalyst, thus accelerating the depletion of HO_2 , however, they can be chelated by
492 OA. OA can also cover the aerosol surface and alter the viscosity of ambient aerosols, thereby
493 decreasing γ , and that more oxidized organic aerosols tend to be highly viscous and thus decrease HO_2
494 uptake coefficients. Results obtained here are in accordance to previous laboratory and modeling studies
495 (Mao et al., 2013a; Lakey et al., 2016b; Lakey et al., 2016a; Takami et al., 2013; Thornton et al., 2008;
496 Hanson et al., 1994), and that the chemical components of ambient aerosols may be internally mixed,
497 as proposed by Takami et al. (2013), which influences the aerosol surface tension and the activity of the
498 free form of the copper ion (i.e., OA and BC) to constrain γ . In contrast to previous studies saying that
499 BC may shrink HO_2 losses onto ambient aerosols (Saathoff et al., 2001; Macintyre and Evans, 2011;
500 Bedjanian et al., 2005), we found BC positively correlated with HO_2 uptake coefficients (0.18), this
501 may be owing to BC can provide active sites thus facilitating the physical uptake of HO_2 . Here, we
502 observed higher γ values (> 0.8) when the mean particle diameter is < 110 nm, identifying the fractional
503 contributions of aerosols in different particle size ranges to k_a and γ is highly desirable in terms of
504 understanding their influence.



505 In summary, the individual chemical components and physical properties of ambient aerosols may
506 dominate γ variation during field campaign; both the metal-catalyzed reactions and the chemical
507 components and their states should be considered to yield more accurate γ values. In future work,
508 improvements to the time-resolution of metal measurements are needed for more precise analysis. For
509 more detailed investigations of HO₂ uptake mechanisms, an offline methodology that can maintain
510 constant chemical compositions or other experimental conditions (such as RH and T) will be useful.
511 The HO₂ loss onto ambient aerosols was identified to have a negligible impact on the O₃ production
512 rate and formation regime owing to the high NO_x concentrations in Yokohama. This process may play
513 a more important role in O₃ formation under low NO_x and high aerosol loading conditions. The results
514 help us to understand the impacts of HO₂ uptake kinetics on chemical transformations in troposphere.

515

516 Appendix:

517 Air mass directions (Figure S1), measurement strategy (Figure S2), a technique combined laser-flash
518 photolysis with laser-induced fluorescence (LFP-LIF), the enrichment of the ambient aerosols, HO₂
519 reactivity of ambient air, correction of gas-phase diffusion for HO₂ uptake coefficient, HO₂ reactivity
520 of ambient gas phase (k_g), examples of HO₂ decay profiles (Figure S3), HO₂ reactivity calibration with
521 different NO₂ concentrations (Figure S4), diurnal trends in individual chemical components of ambient
522 aerosols (Figure S5), diurnal trends in k_a and γ (Figure S6), correlations between measured and modeled
523 γ (Figure S7), time series of the averaged RH and T in ambient air and the reaction cell (Figure S8),
524 dependence of k_a and γ on RH in reaction cell (Figure S9), dependence of k_a and γ on mean particle
525 diameter (Figure S10), dependence of day time LN/Q and LN/Q_without_aerosol on [NO] (Figure
526 S11), profiles of key factors determining XO₂ loss rates and P(O₃) sensitivity (Figure S12), summary
527 of equations and values used for γ modeling (Table S1), summary of equations and values used for XO₂
528 (=HO₂+RO₂) loss and O₃ formation sensitivity regime (Table S1).

529

530 Author contribution



531 J.J., K.M., Y.S., and Y.K. designed the experiments and J.J. and Y.B. carried them out. J.J. did the data
532 analysis and prepared the manuscript with contributions from all co-authors.

533 Competing interests

534 The authors declare that they have no conflict of interest.

535 Data availability

536
537 Data supporting this publication are available upon request for the corresponding author
538 (junzhou@jnu.edu.cn).

539 Acknowledgments

540 This work was supported by the Japan Society for the Promotion of Science (JSPS) KAKENHI Grant
541 Numbers JP16H06305, JP19H04255. Many thanks to Yokohama Environmental Science Research
542 Institute utility during the campaign.

543 References

- 544 Baker, A. R., and Jickells, T. D.: Mineral particle size as a control on aerosol iron solubility, *Geophys.*
545 *Res. Lett.*, 33, 10.1029/2006GL026557, 2006.
- 546 Bedjanian, Y., Lelièvre, S., and Le Bras, G.: Experimental study of the interaction of HO₂ radicals with
547 soot surface, *Phys. Chem. Chem. Phys.*, 7, 334-341, 10.1039/B414217A, 2005.
- 548 Chen, G., Davis, D., Crawford, J., Heikes, B., O'Sullivan, D., Lee, M., Eisele, F., Mauldin, L., Tanner, D.,
549 Collins, J., Barrick, J., Anderson, B., Blake, D., Bradshaw, J., Sandholm, S., Carroll, M., Albercook, G.,
550 and Clarke, A.: An assessment of HO_x chemistry in the tropical pacific boundary layer: comparison of
551 model simulations with observations recorded during PEM Tropics A, *J. Atmos. Chem.*, 38, 317-344,
552 10.1023/A:1006402626288, 2001.
- 553 Cooper, P. L., and Abbatt, J. P. D.: Heterogeneous Interactions of OH and HO₂ Radicals with surfaces
554 characteristic of atmospheric particulate matter, *J. Phys. Chem.*, 100, 2249-2254, 10.1021/jp952142z,
555 1996.
- 556 DeCarlo, P. F., Kimmel, J. R., Trimborn, A., Northway, M. J., Jayne, J. T., Aiken, A. C., Gonin, M., Fuhrer,
557 K., Horvath, T., Docherty, K. S., Worsnop, D. R., and Jimenez, J. L.: Field-Deployable, High-Resolution,
558 Time-of-Flight Aerosol Mass Spectrometer, *Anal. Chem.* 78, 8281-8289, 10.1021/ac061249n, 2006.
- 559 Drinovec, L., Močnik, G., Zotter, P., Prévôt, A. S. H., Ruckstuhl, C., Coz, E., Rupakheti, M., Sciare, J.,
560 Müller, T., Wiedensohler, A., and Hansen, A. D. A.: The "dual-spot" Aethalometer: an improved
561 measurement of aerosol black carbon with real-time loading compensation, *Atmos. Meas. Tech.*, 8,
562 1965-1979, 10.5194/amt-8-1965-2015, 2015.
- 563 Fang, T., Guo, H., Zeng, L., Verma, V., Nenes, A., and Weber, R. J.: Highly acidic ambient particles,
564 soluble metals, and oxidative potential: a link between sulfate and aerosol toxicity, *Environ. Sci.*
565 *Technol.*, 51, 2611-2620, 10.1021/acs.est.6b06151, 2017.



- 566 Finlayson-Pitts, B. J., and Pitts, J. N.: CHAPTER 7 - Chemistry of inorganic nitrogen compounds, in:
567 chemistry of the upper and lower atmosphere, edited by: Finlayson-Pitts, B. J., and Pitts, J. N.,
568 Academic Press, San Diego, 264-293, 2000.
- 569 Fountoukis, C., and Nenes, A.: ISORROPIA II: a computationally efficient thermodynamic equilibrium
570 model for K^+ - Ca^{2+} - Mg^{2+} - NH_4^+ - Na^+ - SO_4^{2-} - NO_3^- - Cl^- - H_2O aerosols, *Atmos. Chem. Phys.*, 7, 4639-4659,
571 10.5194/acp-7-4639-2007, 2007.
- 572 George, I. J., and Abbatt, J. P.: Heterogeneous oxidation of atmospheric aerosol particles by gas-phase
573 radicals, *Nature chem.*, 2, 713-722, 10.1038/nchem.806, 2010.
- 574 George, I. J., Matthews, P. S. J., Whalley, L. K., Brooks, B., Goddard, A., Baeza-Romero, M. T., and Heard,
575 D. E.: Measurements of uptake coefficients for heterogeneous loss of HO_2 onto submicron inorganic
576 salt aerosols, *Phys. Chem. Chem. Phys.*, 15, 12829-12845, 10.1039/C3CP51831K, 2013.
- 577 Gershenzon, Y. M., Grigorieva, V. M., Ivanov, A. V., and Remorov, R. G.: O_3 and OH Sensitivity to
578 heterogeneous sinks of HO and CH_3O_2 on aerosol particles, *Faraday Discuss.*, 100, 83-100,
579 10.1039/FD9950000083, 1995.
- 580 George, C., Ammann, M., and Volkamer, R.: Heterogeneous photochemistry of imidazole-2-
581 carboxaldehyde: HO_2 radical formation and aerosol growth, *Atmos. Chem. Phys.*, 16, 11823-11836,
582 10.5194/acp-16-11823-2016, 2016.
- 583 Gonzalez, J., Torrent-Sucarrat, M., and Anglada, J. M.: The reactions of SO_3 with HO_2 radical and H_2O ·
584 HO_2 radical complex. Theoretical study on the atmospheric formation of HSO_5 and H_2SO_4 , *Phys. Chem.*
585 *Chem. Phys.*, 12, 2116-2125, 10.1039/B916659A, 2010.
- 586 González Palacios, L., Corral Arroyo, P., Aregahegn, K. Z., Steimer, S. S., Bartels-Rausch, T., Nozière, B.,
587 Guieu, C., Chester, R., Nimmo, M., Martin, J. M., Guerzoni, S., Nicolas, E., Mateu, J., and Keyse, S.:
588 Atmospheric input of dissolved and particulate metals to the northwestern Mediterranean, *Deep Sea*
589 *Res. (2 Top. Stud. Oceanogr.)*, 44, 655-674, 10.1016/S0967-0645(97)88508-6, 1997.
- 590 Guo, J., Tilgner, A., Yeung, C., Wang, Z., Louie, P. K. K., Luk, C. W. Y., Xu, Z., Yuan, C., Gao, Y., Poon, S.,
591 Herrmann, H., Lee, S., Lam, K. S., and Wang, T.: Atmospheric peroxides in a polluted subtropical
592 environment: seasonal variation, sources and sinks, and importance of heterogeneous processes,
593 *Environ. Sci. Technol.*, 48, 1443-1450, 10.1021/es403229x, 2014.
- 594 Guo, J., Wang, Z., Tao, W., and Zhang, X.: Theoretical evaluation of different factors affecting the HO_2
595 uptake coefficient driven by aqueous-phase first-order loss reaction, *Sci. Total Environ.*, 683, 146-153,
596 10.1016/j.scitotenv.2019.05.237, 2019.
- 597 Halstead, M. J. R., Cunninghame, R. G., and Hunter, K. A.: Wet deposition of trace metals to a remote
598 site in Fiordland, New Zealand, *Atmos. Environ.*, 34, 665-676, 10.1016/S1352-2310(99)00185-5, 2000.
- 599 Hanson, D. R., Burkholder, J. B., Howard, C. J., and Ravishankara, A. R.: Measurement of hydroxyl and
600 hydroperoxy radical uptake coefficients on water and sulfuric acid surfaces, *J. Phys. Chem.*, 96, 4979-
601 4985, 10.1021/j100191a046, 1992.
- 602 Hanson, D. R., Ravishankara, A. R., and Solomon, S.: Heterogeneous reactions in sulfuric acid aerosols:
603 A framework for model calculations, *J. Geophys. Res. Atmos.*, 99, 3615-3629, 10.1029/93jd02932,
604 1994.
- 605 Heard, D. E., and Pilling, M. J.: Measurement of OH and HO_2 in the Troposphere, *Chem. Rev.*, 103,
606 5163-5198, 10.1021/cr020522s, 2003.
- 607 Hennigan, C. J., Izumi, J., Sullivan, A. P., Weber, R. J., and Nenes, A.: A critical evaluation of proxy
608 methods used to estimate the acidity of atmospheric particles, *Atmos. Chem. Phys.*, 15, 2775-2790,
609 10.5194/acp-15-2775-2015, 2015.
- 610 Hofmann, H., Hoffmann, P., and Lieser, K. H.: Transition metals in atmospheric aqueous samples,
611 analytical determination and speciation, *Fresen. J. Anal. Chem.*, 340, 591-597, 10.1007/BF00322435,
612 1991.
- 613 Hsu, S.-C., Wong, G. T. F., Gong, G.-C., Shiah, F.-K., Huang, Y.-T., Kao, S.-J., Tsai, F., Candice Lung, S.-C.,
614 Lin, F.-J., Lin, I. I., Hung, C.-C., and Tseng, C.-M.: Sources, solubility, and dry deposition of aerosol trace
615 elements over the East China Sea, *Mar. Chem.* 120, 116-127, 10.1016/j.marchem.2008.10.003, 2010.



- 616 J. Creasey, D., A. Halford-Maw, P., E. Heard, D., J. Pilling, M., and J. Whitaker, B.: Implementation and
617 initial deployment of a field instrument for measurement of OH and HO₂ in the troposphere by laser-
618 induced fluorescence, *J. Chem. Soc., Faraday Trans. 93*, 2907-2913, 10.1039/A701469D, 1997.
- 619 George, I. J., Slowik, J., and Abbatt, J.: Chemical aging of ambient organic aerosol from heterogeneous
620 reaction with hydroxyl radicals, *Geophys. Res. Lett.*, 35, L13811, 10.1029/2008GL033884, 2008.
- 621 Jacob, D. J.: Heterogeneous chemistry and tropospheric ozone, *Atmos. Environ.*, 34, 2131-2159,
622 10.1016/S1352-2310(99)00462-8, 2000.
- 623 Jaeglé, L., Jacob, D. J., Brune, W. H., Faloon, I., Tan, D., Heikes, B. G., Kondo, Y., Sachse, G. W.,
624 Anderson, B., Gregory, G. L., Singh, H. B., Poeschel, R., Ferry, G., Blake, D. R., and Shetter, R. E.:
625 Photochemistry of HO_x in the upper troposphere at northern midlatitudes, *J. Geophys. Res. Atmos.*,
626 105, 3877-3892, doi:10.1029/1999JD901016, 2000.
- 627 Kanaya, Y., Cao, R., Akimoto, H., Fukuda, M., Komazaki, Y., Yokouchi, Y., Koike, M., Tanimoto, H.,
628 Takegawa, N., and Kondo, Y.: Urban photochemistry in central Tokyo: 1. Observed and modeled OH
629 and HO₂ radical concentrations during the winter and summer of 2004, *J. Geophys. Res. Atmos.*, 112,
630 10.1029/2007jd008670, 2007a.
- 631 Kanaya, Y., Cao, R., Kato, S., Miyakawa, Y., Kajii, Y., Tanimoto, H., Yokouchi, Y., Mochida, M., Kawamura,
632 K., and Akimoto, H.: Chemistry of OH and HO₂ radicals observed at Rishiri Island, Japan, in September
633 2003: Missing daytime sink of HO₂ and positive nighttime correlations with monoterpenes, 112,
634 10.1029/2006jd007987, 2007b.
- 635 Lakey, P. S. J., George, I. J., Whalley, L. K., Baeza-Romero, M. T., and Heard, D. E.: Measurements of
636 the HO₂ uptake coefficients onto single component organic aerosols, *Environ. Sci. Technol.*, 49, 4878-
637 4885, 10.1021/acs.est.5b00948, 2015.
- 638 Lakey, P. S. J., Berkemeier, T., Krapf, M., Dommen, J., Steimer, S. S., Whalley, L. K., Ingham, T., Baeza-
639 Romero, M. T., Pöschl, U., Shiraiwa, M., Ammann, M., and Heard, D. E.: The effect of viscosity and
640 diffusion on the HO₂ uptake by sucrose and secondary organic aerosol particles, *Atmos. Chem. Phys.*,
641 16, 13035-13047, 10.5194/acp-16-13035-2016, 2016a.
- 642 Lakey, P. S. J., George, I. J., Baeza-Romero, M. T., Whalley, L. K., and Heard, D. E.: Organics substantially
643 reduce HO₂ uptake onto aerosols containing transition metal ions, *J. Phys. Chem. A*, 120, 1421-1430,
644 10.1021/acs.jpca.5b06316, 2016b.
- 645 Logan, J. A., Prather, M. J., Wofsy, S. C., and McElroy, M. B.: Tropospheric chemistry: A global
646 perspective, 86, 7210-7254, 10.1029/JC086iC08p07210, 1981.
- 647 Loukhovitskaya, E., Bedjanian, Y., Morozov, I., and Le Bras, G.: Laboratory study of the interaction of
648 HO₂ radicals with the NaCl, NaBr, MgCl₂·6H₂O and sea salt surfaces, *Phys. Chem. Chem. Phys.*, 11,
649 7896-7905, 10.1039/B906300E, 2009.
- 650 Macintyre, H. L., and Evans, M. J.: Parameterisation and impact of aerosol uptake of HO₂ on a global
651 tropospheric model, *Atmos. Chem. Phys.*, 11, 10965-10974, 10.5194/acp-11-10965-2011, 2011.
- 652 Manoj, S. V., Mishra, C. D., Sharma, M., Rani, A., Jain, R., Bansal, S. P., and Gupta, K. S.: Iron, manganese
653 and copper concentrations in wet precipitations and kinetics of the oxidation of SO₂ in rain water at
654 two urban sites, Jaipur and Kota, in Western India, *Atmos. Environ.*, 34, 4479-4486, 10.1016/S1352-
655 2310(00)00117-5, 2000.
- 656 Mao, J., Jacob, D. J., Evans, M. J., Olson, J. R., Ren, X., Brune, W. H., Clair, J. M. S., Crouse, J. D., Spencer,
657 K. M., Beaver, M. R., Wennberg, P. O., Cubison, M. J., Jimenez, J. L., Fried, A., Weibring, P., Walega, J.
658 G., Hall, S. R., Weinheimer, A. J., Cohen, R. C., Chen, G., Crawford, J. H., McNaughton, C., Clarke, A. D.,
659 Jaeglé, L., Fisher, J. A., Yantosca, R. M., Le Sager, P., and Carouge, C.: Chemistry of hydrogen oxide
660 radicals (HO_x) in the Arctic troposphere in spring, *Atmos. Chem. Phys.*, 10, 5823-5838, 10.5194/acp-
661 10-5823-2010, 2010.
- 662 Mao, J., Fan, S., Jacob, D. J., and Travis, K. R.: Radical loss in the atmosphere from Cu-Fe redox coupling
663 in aerosols, *Atmos. Chem. Phys.*, 13, 509-519, 10.5194/acp-13-509-2013, 2013a.
- 664 Mao, J., Paulot, F., Jacob, D. J., Cohen, R. C., Crouse, J. D., Wennberg, P. O., Keller, C. A., Hudman, R.
665 C., Barkley, M. P., and Horowitz, L. W.: Ozone and organic nitrates over the eastern United States:



- 666 Sensitivity to isoprene chemistry, *J. Geophys. Res. Atmos.*, **118**, 11,256-211,268, 10.1002/jgrd.50817,
667 2013b.
- 668 Martínez, M., Harder, H., Kovacs, T. A., Simpas, J. B., Bassis, J., Leshner, R. L., Brune, W., Frost, G.,
669 Williams, E., Stroud, C., Jobson, B., Roberts, J. M., Hall, S., Shetter, R., Wert, B. P., Fried, A., Alicke, B.,
670 Stutz, J., Young, V., White, A., and Zamora, R. J.: OH and HO₂ concentrations, sources, and loss rates
671 during the Southern Oxidants Study in Nashville, Tennessee, summer 1999, *J. Geophys. Res.*, **108**, 2003.
672 Matthews, P. S. J., Baeza-Romero, M. T., Whalley, L. K., and Heard, D. E.: Uptake of HO₂ radicals onto
673 Arizona test dust particles using an aerosol flow tube, *Atmos. Chem. Phys.*, **14**, 7397-7408,
674 10.5194/acp-14-7397-2014, 2014.
- 675 Millán, L., Wang, S., Livesey, N., Kinnison, D., Sagawa, H., and Kasai, Y.: Stratospheric and mesospheric
676 HO₂ observations from the Aura Microwave Limb Sounder, *Atmos. Chem. Phys.*, **15**, 2889-2902,
677 10.5194/acp-15-2889-2015, 2015.
- 678 Miyazaki, K., Nakashima, Y., Schoemaeker, C., Fittschen, C., and Kajii, Y.: Note: A laser-flash photolysis
679 and laser-induced fluorescence detection technique for measuring total HO₂ reactivity in ambient air,
680 *Rev. Sci. Instrum.*, **84**, 076106, 10.1063/1.4812634, 2013.
- 681 Moon, D. R.; Taverna, G. S.; Anduix-Canto, C.; Ingham, T.; Chipperfield, M. P.; Seakins, P. W.; Baeza-
682 Romero, M. T.; Heard, D. E., Heterogeneous reaction of HO₂ with airborne TiO₂ particles and its
683 implication for climate change mitigation strategies. *Atmos. Chem. Phys.* **2018**, **18**, (1), 327-338.
- 684 Morita, A., Kanaya, Y., and Francisco, J. S.: Uptake of the HO₂ radical by water: Molecular dynamics
685 calculations and their implications for atmospheric modeling, *J. Geophys. Res. Atmos.*, **109**,
686 10.1029/2003jd004240, 2004.
- 687 Mozurkewich, M., McMurry, P. H., Gupta, A., and Calvert, J. G.: Mass accommodation coefficient for
688 HO₂ radicals on aqueous particles, *J. Geophys. Res. Atmos.*, **92**, 4163-4170, 10.1029/JD092iD04p04163,
689 1987.
- 690 Ng, N. L., Canagaratna, M. R., Jimenez, J. L., Chhabra, P. S., Seinfeld, J. H., and Worsnop, D. R.: Changes
691 in organic aerosol composition with aging inferred from aerosol mass spectra, *Atmos. Chem. Phys.*,
692 **11**, 6465-6474, 10.5194/acp-11-6465-2011, 2011.
- 693 Oakes, M., Weber, R. J., Lai, B., Russell, A., and Ingall, E. D.: Characterization of iron speciation in urban
694 and rural single particles using XANES spectroscopy and micro X-ray fluorescence measurements:
695 investigating the relationship between speciation and fractional iron solubility, *Atmos. Chem. Phys.*,
696 **12**, 745-756, 10.5194/acp-12-745-2012, 2012.
- 697 Remorov, R. G., Gershenzon, Y. M., Molina, L. T., and Molina, M. J.: Kinetics and mechanism of HO₂
698 uptake on solid NaCl, *J. Phys. Chem. A*, **106**, 4558-4565, 10.1021/jp013179o, 2002.
- 699 Ross, H. B., and Noone, K. J.: A numerical investigation of the destruction of peroxy radical by Cu ion
700 catalysed reactions on atmospheric particles, *J. Atmos. Chem.*, **12**, 121-136, 10.1007/BF00115775,
701 1991.
- 702 Saathoff, H., Naumann, K.-H., Riemer, N., Kamm, S., Möhler, O., Schurath, U., Vogel, H., and Vogel, B.:
703 The loss of NO₂, HNO₃, NO₃/N₂O₅, and HO₂/HOONO₂ on soot aerosol: A chamber and modeling study,
704 *Geophys. Res. Lett.*, **28**, 1957-1960, 10.1029/2000gl012619, 2001.
- 705 Sadanaga, Y., Yoshino, A., Watanabe, K., Yoshioka, A., Wakazono, Y., Kanaya, Y., and Kajii, Y.:
706 Development of a measurement system of OH reactivity in the atmosphere by using a laser-induced
707 pump and probe technique, *Rev. Sci. Instrum.*, **75**, 2648-2655, 10.1063/1.1775311, 2004.
- 708 Sakamoto, Y., Zhou, J., Kohno, N., Nakagawa, M., Hirokawa, J., and Kajii, Y.: Kinetics study of OH uptake
709 onto deliquesced NaCl particles by combining Laser Photolysis and Laser-Induced Fluorescence, *J. Phys.*
710 *Chem. Lett.*, **9**, 4115-4119, 10.1021/acs.jpcclett.8b01725, 2018.
- 711 Sakamoto, Y., Sadanaga, Y., Li, J., Matsuoka, K., Takemura, M., Fujii, T., Nakagawa, M., Kohno, N.,
712 Nakashima, Y., Sato, K., Nakayama, T., Kato, S., Takami, A., Yoshino, A., Murano, K., and Kajii, Y.:
713 Relative and absolute sensitivity analysis on ozone production in Tsukuba, a city in Japan, *Environ. Sci.*
714 *Technol.*, **53**, 13629-13635, 10.1021/acs.est.9b03542, 2019.
- 715 Sedlak, D. L., and Hoigné, J.: The role of copper and oxalate in the redox cycling of iron in atmospheric
716 waters, *Atmos. Environ., Part A. General Topics*, **27**, 2173-2185, 10.1016/0960-1686(93)90047-3, 1993.



- 717 Siefert, R. L., Johansen, A. M., Hoffmann, M. R., and Pehkonen, S. O.: Measurements of trace metal
718 (Fe, Cu, Mn, Cr) oxidation states in fog and stratus clouds, *J. Air Waste Manage.*, **48**, 128-143,
719 10.1080/10473289.1998.10463659, 1998.
- 720 Sommariva, R., Haggerstone, A. L., Carpenter, L. J., Carslaw, N., Creasey, D. J., Heard, D. E., Lee, J. D.,
721 Lewis, A. C., Pilling, M. J., and Zádor, J.: OH and HO₂ chemistry in clean marine air during SOAPEX-2,
722 *Atmos. Chem. Phys.*, **4**, 839-856, 10.5194/acp-4-839-2004, 2004.
- 723 Song, H., Chen, X., Lu, K., Zou, Q., Tan, Z., Fuchs, H., Wiedensohler, A., Zheng, M., Wahner, A., Kiendler-
724 Scharr, A., and Zhang, Y.: Influence of aerosol copper on HO₂ uptake: A novel parameterized equation,
725 *Atmos. Chem. Phys. Discuss.*, 2020, 1-23, 10.5194/acp-2020-218, 2020.
- 726 Stadtler, S., Simpson, D., Schröder, S., Taraborrelli, D., Bott, A., and Schultz, M.: Ozone impacts of gas-
727 aerosol uptake in global chemistry transport models, *Atmos. Chem. Phys.*, **18**, 3147-3171,
728 10.5194/acp-18-3147-2018, 2018.
- 729 Stone, D., Whalley, L. K., and Heard, D. E.: Tropospheric OH and HO₂ radicals: field measurements and
730 model comparisons, *Chem. Soc. Rev.*, **41**, 6348-6404, 10.1039/C2CS35140D, 2012.
- 731 Takami, A., Mayama, N., Sakamoto, T., Ohishi, K., Irei, S., Yoshino, A., Hatakeyama, S., Murano, K.,
732 Sadanaga, Y., Bandow, H., Misawa, K., and Fujii, M.: Structural analysis of aerosol particles by
733 microscopic observation using a time-of-flight secondary ion mass spectrometer, *J. Geophys. Res.*
734 *Atmos.*, **118**, 6726-6737, 10.1002/jgrd.50477, 2013.
- 735 Taketani, F., Kanaya, Y., and Akimoto, H.: Kinetics of heterogeneous reactions of HO₂ radical at
736 ambient concentration levels with (NH₄)₂SO₄ and NaCl aerosol particles, *J. Phys. Chem. A*, **112**, 2370-
737 2377, 10.1021/jp0769936, 2008.
- 738 Taketani, F.; Kanaya, Y.; Akimoto, H., Heterogeneous loss of HO₂ by KCl, synthetic sea salt, and natural
739 seawater aerosol particles. *Atmospheric Environment* **2009**, *43*, (9), 1660-1665.
- 740 Taketani, F., Kanaya, Y., Pochanart, P., Liu, Y., Li, J., Okuzawa, K., Kawamura, K., Wang, Z., and Akimoto,
741 H.: Measurement of overall uptake coefficients for HO₂ radicals by aerosol particles sampled from
742 ambient air at Mts. Tai and Mang (China), *Atmos. Chem. Phys.*, **12**, 11907-11916, 10.5194/acp-12-
743 11907-2012, 2012.
- 744 Thornton, J., and Abbatt, J. P. D.: Measurements of HO₂ uptake to aqueous aerosol: Mass
745 accommodation coefficients and net reactive loss, *J. Geophys. Res. Atmos.*, **110**,
746 10.1029/2004jd005402, 2005.
- 747 Thornton, J. A., Jaeglé, L., and McNeill, V. F.: Assessing known pathways for HO₂ loss in aqueous
748 atmospheric aerosols: Regional and global impacts on tropospheric oxidants, *J. Geophys. Res. Atmos.*,
749 **113**, 10.1029/2007jd009236, 2008.
- 750 Tie, X., Brasseur, G., Emmons, L., Horowitz, L., and Kinnison, D.: Effects of aerosols on tropospheric
751 oxidants: A global model study, *J. Geophys. Res. Atmos.*, **106**, 22931-22964, 10.1029/2001JD900206,
752 2001.
- 753 Wang, Y., Arellanes, C., Curtis, D. B., and Paulson, S. E.: Probing the source of hydrogen peroxide
754 associated with coarse mode aerosol particles in southern California, *Environ. Sci. Technol.*, **44**, 4070-
755 4075, 10.1021/es100593k, 2010.
- 756 Whalley, L. K., Furneaux, K. L., Goddard, A., Lee, J. D., Mahajan, A., Oetjen, H., Read, K. A., Kaaden, N.,
757 Carpenter, L. J., Lewis, A. C., Plane, J. M. C., Saltzman, E. S., Wiedensohler, A., and Heard, D. E.: The
758 chemistry of OH and HO₂ radicals in the boundary layer over the tropical Atlantic Ocean, *Atmos. Chem.*
759 *Phys.*, **10**, 1555-1576, 10.5194/acp-10-1555-2010, 2010.
- 760 Wilkinson, J., Reynolds, B., Neal, C., Hill, S., Neal, M., and Harrow, M.: Major, minor and trace element
761 composition of cloudwater and rainwater at Plynlimon, *Hydrol. Earth Syst. Sci.*, **1**, 557-569,
762 10.5194/hess-1-557-1997, 1997.
- 763 Zhou, J., Elser, M., Huang, R. J., Krapf, M., Fröhlich, R., Bhattu, D., Stefenelli, G., Zotter, P., Bruns, E. A.,
764 Pieber, S. M., Ni, H., Wang, Q., Wang, Y., Zhou, Y., Chen, C., Xiao, M., Slowik, J. G., Brown, S., Cassagnes,
765 L. E., Daellenbach, K. R., Nussbaumer, T., Geiser, M., Prévôt, A. S. H., El-Haddad, I., Cao, J.,
766 Baltensperger, U., and Dommen, J.: Predominance of secondary organic aerosol to particle-bound



767 reactive oxygen species activity in fine ambient aerosol, *Atmos. Chem. Phys.*, **19**, 14703-14720,
768 10.5194/acp-19-14703-2019, 2019a.
769 Zhou, J., Murano, K., Kohno, N., Sakamoto, Y., and Kajii, Y.: Real-time quantification of the total HO₂
770 reactivity of ambient air and HO₂ uptake kinetics onto ambient aerosols in Kyoto (Japan), *Atmosph.*
771 *Environ.*, 117189, 10.1016/j.atmosenv.2019.117189, 2019b.

772